

A [2]pseudorotaxane based on a pillar[6]arene and its application in the construction of metallosupramolecular polymer

Danyu Xia,^{*a} Xiaoqing Lv,^a Kexian Chen,^{*c} and Pi Wang^{*b}

^aScientific Instrument Center, Shanxi University, Taiyuan, 030006, P. R. China; E-mail:

danyuxia@sxu.edu.cn

^bMinistry of Education Key Laboratory of Interface Science and Engineering in Advanced
Materials, Taiyuan University of Technology, Taiyuan, 030024, P.R. China; E-mail:

wangpi@tyut.edu.cn

^cSchool of Food Science and Biotechnology, Zhejiang Gongshang University, Hangzhou,
310018, PR China

Electronic Supplementary Information (9 pages)

1.	<i>Materials and Methods</i>	S2
2.	<i>Variable-temperature ¹H NMR spectra of P6⊃G</i>	S2
3.	<i>Partial 2D NOESY spectrum of P6⊃G</i>	S2
4.	<i>Stoichiometry and association constant determination for the complexation between P6 and G</i>	S3
5.	<i>Stoichiometry determination for the between the coordination between complex P6⊃G and Ag⁺</i>	S5
6.	<i>¹H NMR titration experiments of Ag⁺ to P6⊃G</i>	S6
7.	<i>Diffusion coefficient D of P6 + G and P6 + G + Ag⁺</i>	S6
8.	<i>DLS data of P6 + G and P6 + G + Ag⁺</i>	S7
9.	<i>Optical microscope image of the polypseudorotaxane</i>	S8
10.	<i>Powder X-ray diffraction (XRD) analysis of the polypseudorotaxane</i>	S8
	<i>References</i>	S9

1. Materials and Methods:

Compound (**P6**)^{S1} and (**G**)^{S2} were synthesized according to literature procedures. All reagents were commercially available and used as supplied without further purification. Solvents were either employed as purchased or dried according to procedures described in the literature. NMR spectra were recorded with a Bruker Avance DMX 500 spectrophotometer or a Bruker Avance DMX 400 spectrophotometer. UV-vis spectra were taken on a Perkin-Elmer Lambda 35 UV-vis spectrophotometer. Dynamic light scattering was carried out on a Malvern Nanosizer S instrument at room temperature. XRD were performed with a Bruker D2 PHASER. Optical microscope image was made by a Bruker Multi-Mode 8.0 AFM instrument.

2. Variable-temperature ¹H NMR spectra of **P6**↔**G**

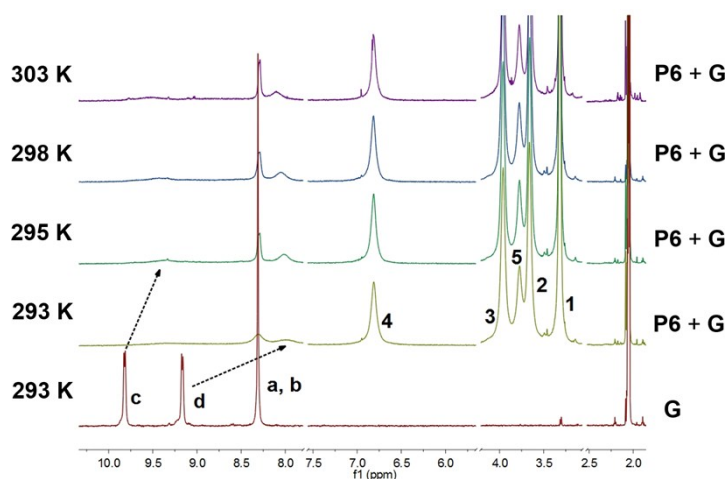


Figure S1 Variable-temperature ¹H NMR spectra (500 MHz, CD₃COCD₃) of an equimolar solution of **P6** and **G** (5.00 mM).

3. Partial 2D NOESY spectrum of **P6**↔**G**

2D NOESY experiment was employed to study the relative positions of the components in complex **P6**↔**G**. NOE correlation signals were observed between protons H_a and H_b of **G** and proton H₁, H₂, H₃, H₄ of **P6** (Figure S2, A, B, C, D) and between protons H_d of **G** and proton H₄ of **P6** (Figure S2, E).

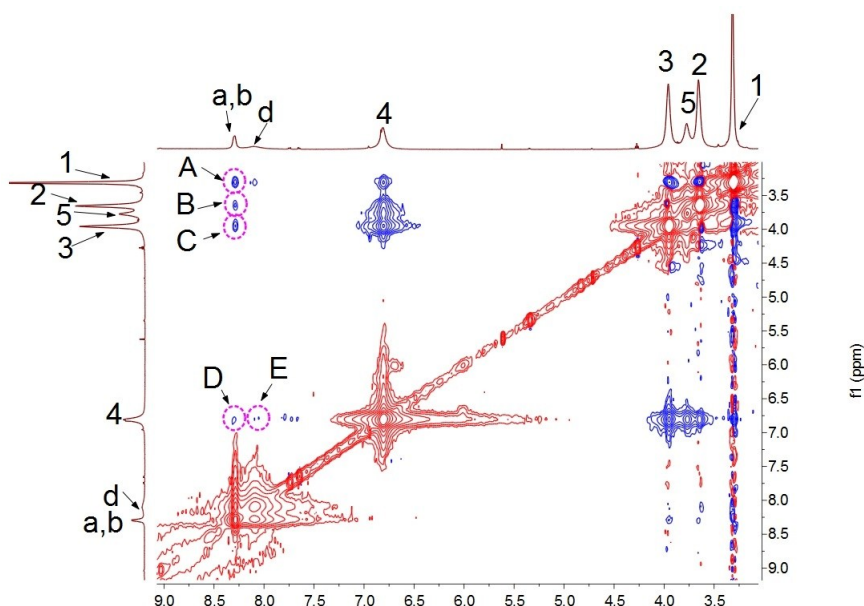


Figure S2 Partial 2D NOESY spectrum (500 MHz, CD_3COCD_3 , room temperature) of an equimolar mixture **P6** and **G** (5.00 mM).

4. Stoichiometry and association constant determination for the complexation between **P6** and **G**

The association constant of complex **P6**⊃**G** was determined by probing the charge-transfer band of the complex by UV-vis spectroscopy and employing a titration method. Progressive addition of a solution with high guest **G** concentration (1.0×10^{-2} M) and low host **P6** concentration (1.0×10^{-4} M) to a solution with the same concentration of host **P6** resulted in an increase of the intensity of the charge-transfer band of the complex. Treatment of the collected absorbance data with a non-linear curve-fitting program afforded the corresponding association constant (K_a): (3.58 ± 0.13) $\times 10^3 \text{ M}^{-1}$ for **P6**⊃**G** in acetone.

The non-linear curve-fitting was based on the equation:^{S3}

$$A = (A_\infty/[H]_0) (0.5[G]_0 + 0.5([H]_0 + 1/K_a) - (0.5 ([G]_0^2 + (2[G]_0(1/K_a - [H]_0)) + (1/K_a + [H]_0)^2)^{0.5})) \quad (\text{Eq. S1})$$

Where A is the absorption intensity of the charge-transfer band at $[G]_0$, A_∞ is the absorption intensity of the charge-transfer band when the host is completely complexed, $[H]_0$ is the fixed initial concentration of the host **P6**, and $[G]_0$ is the varying concentration of the guest **G**.

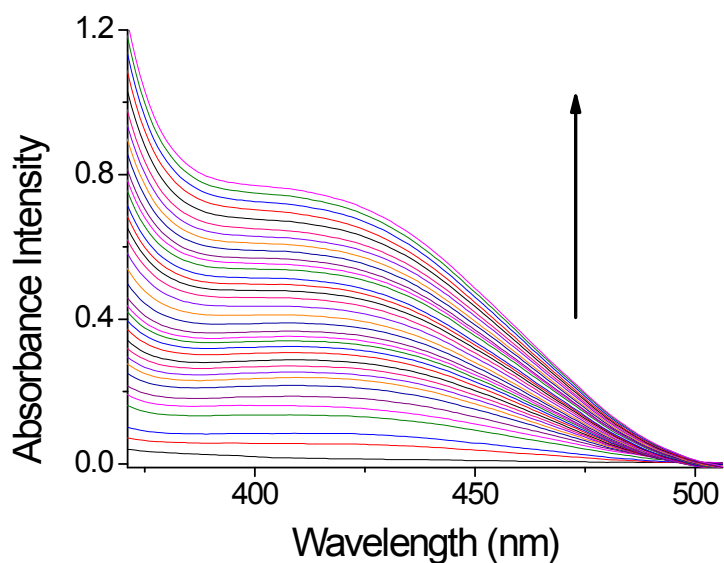


Figure S3 The absorption spectral changes of **P6** (1.0×10^{-4} M) upon addition of **G**. The concentrations of **G** were 0.00 mM, 0.00999 mM, 0.00200 mM, 0.0398 mM, 0.0498 mM, 0.0596 mM, 0.0794 mM, 0.0990 mM, 0.119 mM, 0.138 mM, 0.157 mM, 0.177 mM, 0.196 mM, 0.215 mM, 0.234 mM, 0.253 mM, 0.291 mM, 0.329 mM, 0.366 mM, 0.403 mM, 0.440 mM, 0.476 mM, 0.512 mM, 0.548 mM, 0.584 mM, 0.619 mM, 0.672 mM, 0.724 mM, 0.775 mM, 0.842 mM, 0.909 mM, 0.975 mM, 1.040 Mm and 1.170 mM.

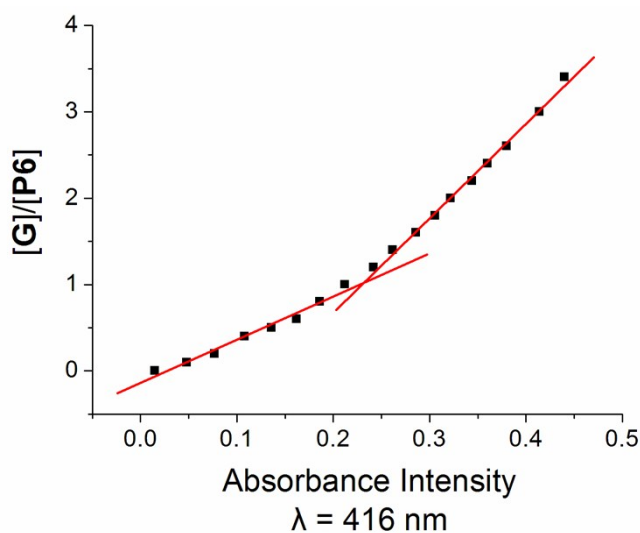


Figure S4 Mole ratio plot for the complexation between **P6** and **G**, indicating a 1:1 stoichiometry.

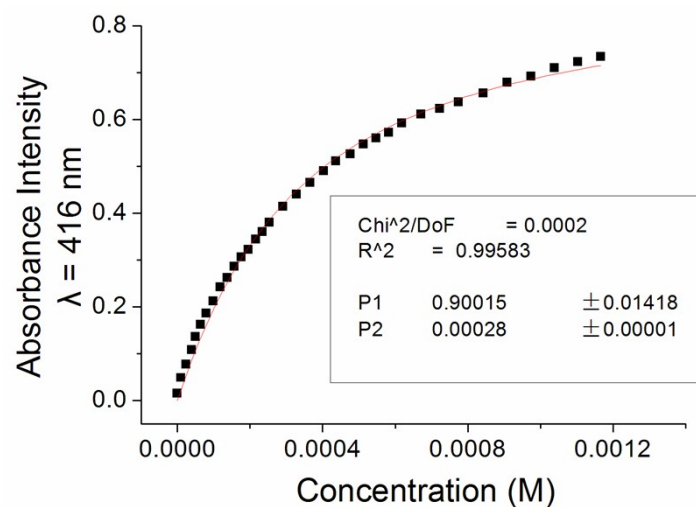


Figure S5 The absorbance intensity changes at $\lambda = 416$ nm upon addition of **G** (from 0 to 1.17×10^{-3} M). The red solid line was obtained from the non-linear curve-fitting using Eq. S1.

5. Stoichiometry determination for the between the coordination between complex **P6**⊃**G** and Ag^+

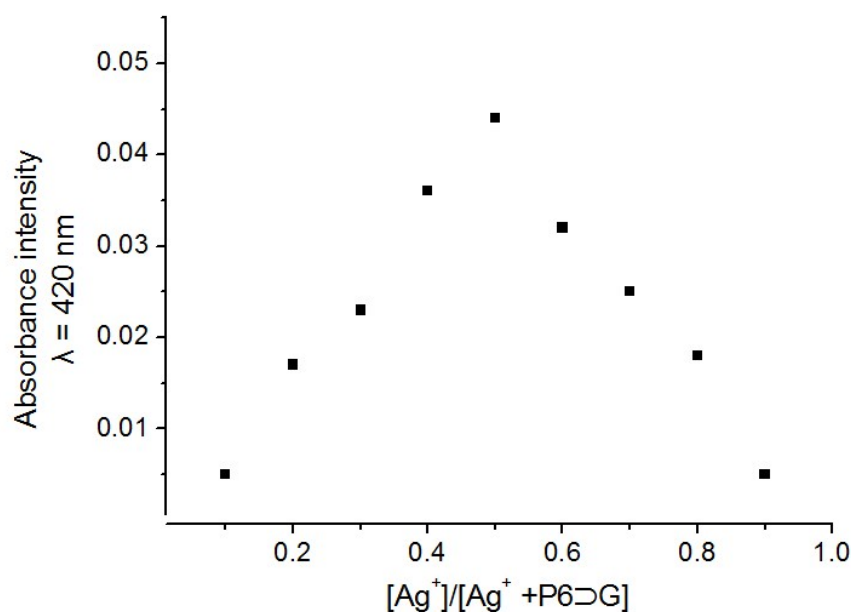


Figure S6 Job plot for the coordination between Ag^+ and **P6**⊃**G**, indicating a 1:1 stoichiometry. The total concentration of Ag^+ and **P6**⊃**G** was 0.0500 mM. The concentration of Ag^+ was from 0.00500 mM to 0.0450 mM.

6. ^1H NMR titration experiments of Ag^+ to $\text{P6} \supset \text{G}$

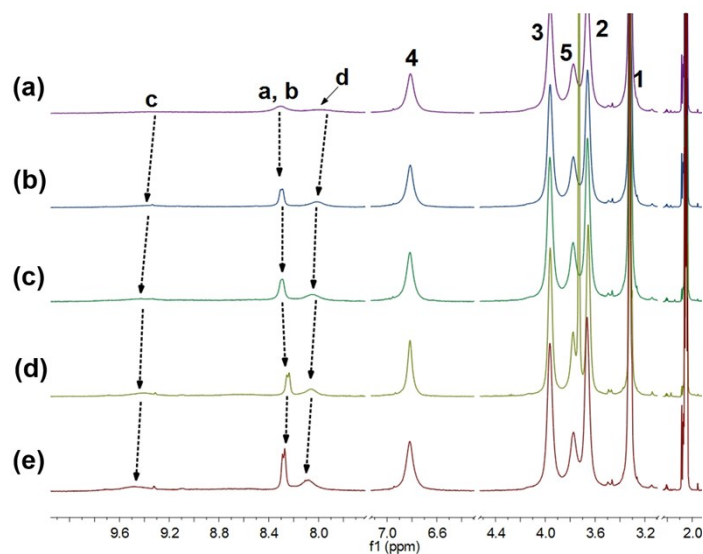


Figure S7 Partial ^1H NMR spectra (500 MHz, CD_3COCD_3 , room temperature) of equimolar mixture of $\text{P6} + \text{G}$ at a concentration of 5.00 mM with successive addition of AgSbF_6 : a) 0 equiv; b) 0.2 equiv; c) 0.4 equiv; d) 0.8 equiv; e) 1.0 equiv. of AgSbF_6 .

7. Diffusion coefficient D of $\text{P6} + \text{G}$ and $\text{P6} + \text{G} + \text{Ag}^+$

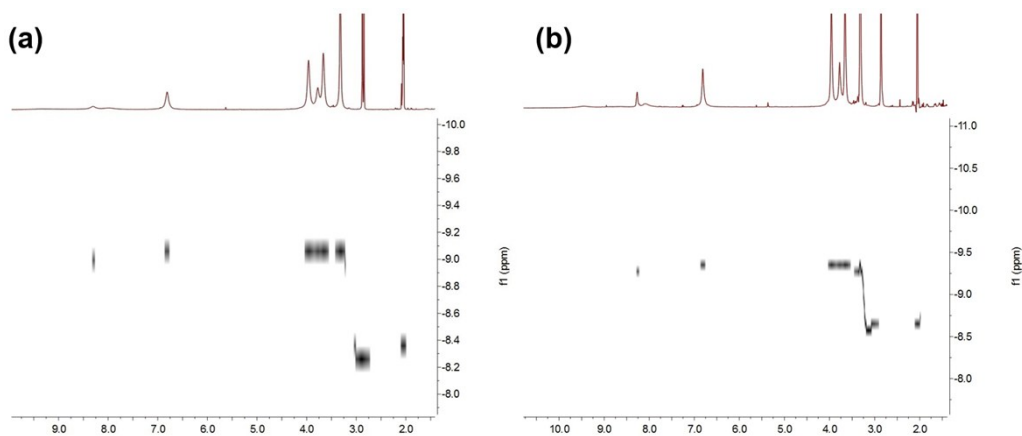


Figure S8 2D DOSY Spectra (500 MHz, CD_3COCD_3 , room temperature.): (a) equimolar mixture of $\text{P6} + \text{G}$ (5.00 mM); (b) equimolar mixture of $\text{P6} + \text{G} + \text{Ag}^+$ (5.00 mM).

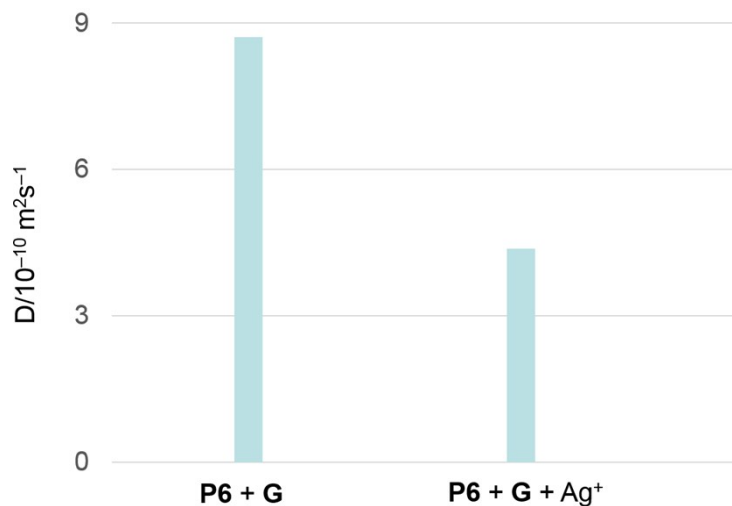


Figure S9 Concentration dependence of diffusion coefficient D (500 MHz, CD_3COCD_3 , room temperature) of equimolar mixtures of **P6 + G** and **P6 + G + Ag⁺** (5.00 mM).

8. DLS data of **P6 + G** and **P6 + G + Ag⁺**

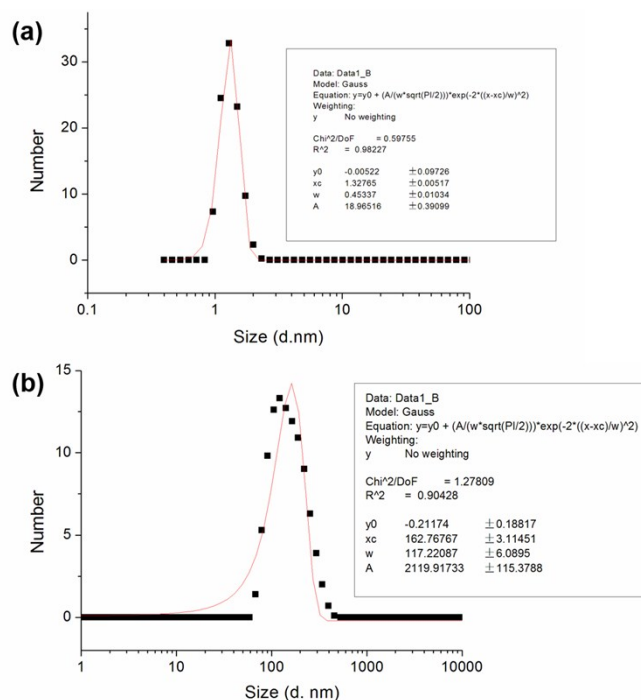


Figure S10 DLS data: (a) **P6+G** (5.00 mM); (b) **P6+G** (5.00 mM) and **Ag⁺** (5.00 mM) in acetone. The red solid lines were obtained from the non-linear curve-fitting using Gaussian distribution.

9. Optical microscope images of the polypseudorotaxane

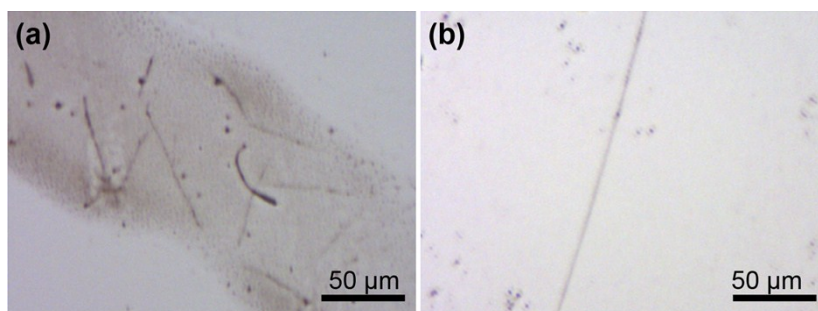


Figure S11 Optical microscope images of the polypseudorotaxane.

10. Powder X-ray diffraction analysis of the polypseudorotaxane

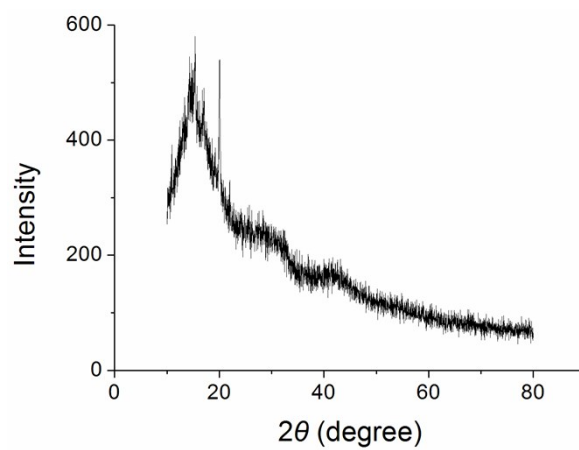


Figure S12 Powder X-ray diffraction analysis of the polypseudorotaxane.

References:

- S1. X. Chi, M. Xue, Y. Ma, X. Yan and F. Huang, *Chem. Commun.*, 2013, **49**, 8175–8177.
- S2. F. Biedermann, O. A. Scherman, *J. Phys. Chem. B*, 2012, **116**, 2842–2849
K. A. Connors, *Binding Constants*; Wiley: New York, 1987; P. S. Corbin, Ph.D. Dissertation, University of Illinois at Urbana-Champaign, Urbana, IL, 1999; P. R. Ashton, R. Ballardini, V. Balzani, M. Belohradsky, M. T. Gandolfi, D. Philp, L. Prodi, F. M. Raymo, M. V. Reddington, N. Spencer, J. F. Stoddart, M. Venturi and D. J. Williams, *J. Am. Chem. Soc.*, 1996, **118**, 4931–4951.
- S3. F. Biedermann, O. A. Scherman, *J. Phys. Chem. B*, 2012, **116**, 2842–2849
K. A. Connors, *Binding Constants*; Wiley: New York, 1987; P. S. Corbin, Ph.D. Dissertation, University of Illinois at Urbana-Champaign, Urbana, IL, 1999; P. R. Ashton, R. Ballardini, V. Balzani, M. Belohradsky, M. T. Gandolfi, D. Philp, L. Prodi, F. M. Raymo, M. V. Reddington, N. Spencer, J. F. Stoddart, M. Venturi and D. J. Williams, *J. Am. Chem. Soc.*, 1996, **118**, 4931–4951.